Research Article | Vol. 28, No. 23 / 9 November 2020 / Optics Express 33921
Optics EXPRESS

# Generation of strong-field spectrally tunable terahertz pulses

A. V. Ovchinnikov,[1,*] O. V. Chefonov,[1] M. B. Agranat,[1] V. E. Fortov,[1] M. Jazbinsek,[2] and C. P. Hauri[3,4,5]

[1]Joint Institute for High Temperatures of RAS, Izhorskaya st. 13 Bd. 2, Moscow 125412, Russia
[2]Zurich University of Applied Sciences (ZHAW), ICP, 8400 Winterthur, Switzerland
[3]Trumpf Schweiz AG, 7214 Gruesch, Switzerland
[4]Paul Scherrer Institute, SwissFEL, 5232 Villigen PSI, Switzerland
[5]École Polytechnique Fédérale de Lausanne, 1015 Lausanne, Switzerland
[*]a.ovtch@gmail.com

**Abstract:** The ideal laser source for nonlinear terahertz spectroscopy offers large versatility delivering both ultra-intense broadband single-cycle pulses and user-selectable multi-cycle pulses at narrow linewidths. Here we show a highly versatile terahertz laser platform providing single-cycle transients with tens of MV/cm peak field as well as spectrally narrow pulses, tunable in bandwidth and central frequency across 5 octaves at several MV/cm field strengths. The compact scheme is based on optical rectification in organic crystals of a temporally modulated laser beam. It allows up to 50 cycles and central frequency tunable from 0.5 to 7 terahertz, with a minimum width of 30 GHz, corresponding to the photon-energy width of $\Delta E$=0.13 meV and the spectroscopic-wavenumber width of $\Delta(\lambda^{-1})$=1.1 cm$^{-1}$. The experimental results are excellently predicted by theoretical modelling. Our table-top source shows similar performances to that of large-scale terahertz facilities but offering in addition more versatility, multi-colour femtosecond pump-probe opportunities and ultralow timing jitter.



## 1. Introduction

Terahertz radiation represents an ideal stimulus for controlling matter in a more advanced way compared to an optical light stimulus. While optical light predominantly interacts with valence electrons, terahertz radiation, defined as the frequency region between 0.1 and 10 terahertz, allows direct and selective access to the numerous low-energy excitations including lattice vibrations, spin waves, molecular rotations, quantum states and the internal excitations of bound electron-hole pairs [1–12]. Recent advances in the available terahertz brightness also enable non-resonant control over matter where the terahertz stimulus acts as ultrafast excitation [13–16]. While the selective control requires narrowband terahertz radiation, the non-resonant excitation relies on intense single-cycle terahertz pulses carrying a (multi-) octave spanning spectrum.

The ideal source for linear and nonlinear terahertz spectroscopy should give the experimenter free control on the number and the period of the electric field oscillations, from one to many cycles, corresponding to broadband or narrowband spectra, and to apply the highest possible electric field strength up to tens of MV/cm. Nowadays different laser driven sources are used to produce single-cycle high-field terahertz pulses. Large terahertz pulse energies (>400 $\mu$J) and MV/cm electric field strengths have been demonstrated by optical rectification in lithium niobite [17–19]. One order larger field strengths reaching tens of MV/cm have become recently available using optical rectification in organic crystals [13,20]. Gas-plasma terahertz sources driven by two-colour laser demonstrated ultrabroadband single-cycle transient with the potential of tens of MV/cm field and energy conversion efficiency of few percent [21–24]. On the other hand, the production of narrowband spectra at high field strength (>0.1 MV/cm) which are tunable across several octaves has remained a formidable challenge. Intense terahertz radiation confined

#405545 https://doi.org/10.1364/OE.405545
Journal © 2020 Received 18 Aug 2020; revised 2 Oct 2020; accepted 17 Oct 2020; published 26 Oct 2020

Optics EXPRESS

in a narrow spectral line is, however, a necessity for ground-breaking investigations in imaging, light-induced electron acceleration and nonlinear selective excitation of resonant modes.

In the past, several schemes for forming tunable narrowband terahertz radiation have been presented. The two main approaches are based on charged particle beams and lasers. Large-size electron accelerators with energy up to several GeV provide terahertz pulses with up to hundreds of μJ by means of transition, edge or free electron lasers (T-FEL) radiation [25–30]. These sources offer only broadband terahertz radiation and the opportunity for tunable narrowband spectral emission is minor. By employing an electron bunch train spectrally confined terahertz radiation with a relative bandwidth $\delta f_{\mathrm{THz}}/f_0$ of typically > 20% could be demonstrated [27]. However, the polarization from this source is radial, which is unfavourable for many experiments as it requires high loss polarization filtering to transform it to a well-defined linearly polarization state. Furthermore, the user accessibility to such large-scale sources is restricted, as the primary usage of these accelerators is different. Dedicated T-FELs deliver radiation of tens of $\mu$J with a relative bandwidth variable between 0.2–5% in the range of ≈0.3–10 THz [31]. Undulator-based sources, such as the T-FELs, deliver multicycle fields with number of oscillation proportional to the undulator periods (typically 10–100) and are not suited for single-cycle terahertz radiation. As terahertz generation starts from noise, the field from T-FELs does not offer a stable absolute phase. This is a particular burden for phase-sensitive experiments at sub-cycle resolution. Furthermore, the synchronization with an external femtosecond laser required for pump-probe experiments requires challenging technology. This kind of system has been recently realized in [32].

Table-top narrowband terahertz sources are realized by employing a molecular gas transition pumped with a powerful $CO_2$ laser [33] or by optical down-conversion of a short-pulse laser using the second-order $\chi^{(2)}$ optical rectification (OR) process in nonlinear crystals [34,35]. While the former is limited in tunability to a set of specific molecular transitions, the latter is typically used for broadband, single-cycle pulse production. However, for OR-based sources, technics for spectral confinement of terahertz radiation have been demonstrated by employing pump pulse shaping technique, but the performance in view of spectral width, tunability of the central frequency and brightness still deviates significantly from T-FEL based sources. Pulse shaping of the pump beam by spatial [36] or spectral [37] control results in narrow terahertz radiation tunable between 0.5–2 THz with a relative spectral bandwidth $\delta f_{\mathrm{THz}}/f_0$ of typically 20–30%. Other schemes employ periodically poled nonlinear crystals with a specially engineered multi-layer structure to generate terahertz pulses at a fixed frequency [38]. Unfortunately, the resulting terahertz pulse energy of typically <100 nJ is not sufficient to initiate nonlinear processes. Similar restrictions for terahertz pulse energy and field hold for narrowband terahertz sources based on beating of two broadband chirped pump pulses either on a dipole antenna [39] via a fast oscillating current induced by the beat frequency or in nonlinear optical crystals [40,41]. A terahertz source with central frequency between 4 and 18 THz and bandwidth of 1 THz, has been demonstrated by difference frequency generation with chirped pulses [42]. A theoretical model of multi-cycle terahertz generation in periodically poled lithium niobate has been reported [43]. Experimental results of narrowband THz pulse generation in the same type of converter medium has been reported at a fixed frequency of 0.361 THz with record pulse energy of 0.6 mJ [44]. The THz radiation driven by two-color laser pulses in gas plasma can be changed from broadband to narrowband when an external magnetic field is applied [45]. Another approach based on phase-matched collinear difference-frequency generation in a single GaSe crystal and continuously tunable in a wide THz range has been demonstrated [46]. A narrow linewidth operation of a THz-wave parametric oscillator was achieved through the use of narrow linewidth laser injection [47]. However, overall, the performance for state-of-the-art laser-based THz sources has been limited so far in terms of the central-frequency tunability at narrow bandwidth, pulse energy and field strength. The scheme presented here overcomes all of these shortcomings.

Optics EXPRESS

In this paper we demonstrate an advanced scheme which provides both intense laser-based terahertz radiation adjustable across a large central frequency range between $f_0$=0.5 and 7 THz and outstanding bandwidth tunability between $\delta f_{\mathrm{THz}}$=0.03 and 5 THz, where $\delta f_{\mathrm{THz}}$ is the full width at half maximum (FWHM) of the THz intensity spectrum. Our approach is based on optical rectification of a temporally modulated chirped pump laser in an organic crystal. The scheme offers continuous tunability from a single to a multi-cycle pulse exceeding 50 periods. It is superior to other laser-based sources in view of efficiency, versatility and tunability as it offers a relative spectral bandwidth $\delta f_{\mathrm{THz}}/f_0$ continuously selectable between 100% and 2.5% (covering the bandwidth $\delta f_{\mathrm{THz}}$ between 0.03 and 5 THz). The presented simple approach can, in principle, be extended towards linewidths of <1%. The present results widen the potential of existing high-power lasers as sources of versatile terahertz radiation and open new opportunities for nonlinear applications with multicycle pulses at MV/cm field strength for time-resolved investigations.

## 2. Experimental setup and theoretical modelling

The experiments were conducted on the Cr:Forsterite chirped-pulse amplification laser at the Joint Institute of High Temperature of the Russian Academy of Science shown in Fig. 1 emitting 120 fs pulses at a wavelength of 1.23 $\mu$m with pulse energy up to 20 mJ and repetition rate of 10 Hz [48].

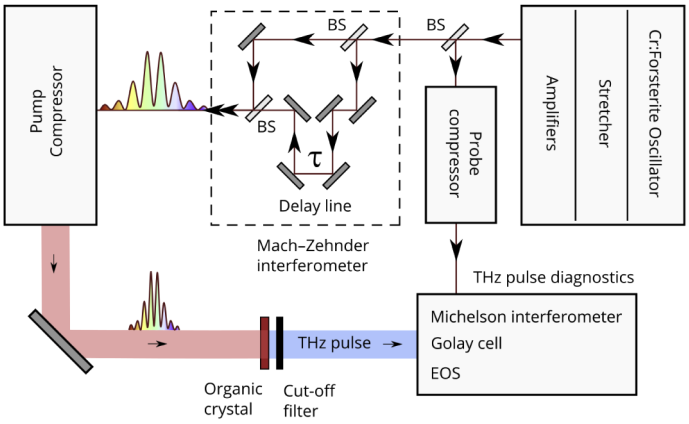


**Fig. 1.** Experimental layout. The amplified laser pulse from a Cr:forsterite chirped pulsed amplification (CPA) laser is split and delayed by means of a Mach Zehnder-type interferometer before re-compression to the few picosecond or femtosecond regime. The beat frequency $f_0$ of the two chirped pulses is selected by varying the delay time $\tau$ of the two paths in the interferometer and the chirp rate $\mu$. BS — beamsplitters. EOS — electro-optic sampling.

During the experiment the laser provides up to 10 mJ pulse energy after compression. The laser spectrum of ≈22 nm (FWHM) is well suited for broadband and efficient optical rectification in the 410 $\mu$m thick organic crystal DSTMS [49] (4-N,N-dimethylamino-4'-N'-methyl-stilbazolium 2,4,6-trimethylbenzenesulfonate) and 450 $\mu$m OH1 (2-(3-(4-Hydroxystyryl)-5,5-dimethylcyclohex-2-enylidene)malononitrile), used in our studies [50,51]. The setup allows for the formation of a pulse replica by means of a Mach-Zehnder type interferometer introducing a time-delayed second pulse at a variable delay $\tau$. As the two co-propagating replicas are stretched in time, a frequency chirp beating occurs in case of temporal overlap. A linearly chirped Gaussian

Optics EXPRESS

laser electric field can be described as:

$$E(t) = \frac{1}{2}E_0 \times \sqrt{\frac{\sigma}{\sigma_n}} \times \exp(-i\omega_0\tau) \times \exp\left(-\frac{t^2}{\sigma_n^2}(1 - i\frac{2}{\mu\sigma^2})\right);$$

with $E_0$ and $\omega_0$ being the field amplitude and the carrier angular frequency, $\mu$ the chirp rate, $\sigma$ and $\sigma_n = \sigma\sqrt{1 + (2/\mu\sigma^2)^2}$ the transform-limited and the chirped 1/e field-half-widths. The highly modulated pulse train is obtained in the experiment by the superposition of two delayed chirped pulses $E(t + \tau/2) + E(t - \tau/2)$ (see Fig. 1). The modulated laser intensity is optically rectified in DSTMS or OH1 organic crystals for multicycle/narrowband terahertz emission.

The generated THz spectral intensity $I_{\mathrm{THz}}(f)$ is proportional to $|H(f,\lambda)|^2$ and $|I_{\mathrm{opt}}(f,\mu,\tau)|^2$ (see Section 3, Eq. (1)). $H(f,\lambda)$ is the optical rectification response function, which takes into account the optical and the THz properties of the particular organic crystal, such as the nonlinear optical coefficient, the velocity matching condition between the optical pump at the wavelength $\lambda$ and the terahertz beam at the frequency $f$ and the optical/terahertz absorption according to Eq. (2) in Section 3. $I_{\mathrm{opt}}(f,\mu,\tau)$ is simply the Fourier transform of the modulated optical pump intensity and depends on the chirp rate $\mu$ and the delay time $\tau$ (see Section 3, Eqs. (3), (4), (5)). The generated narrowband terahertz spectrum is centred at the laser beating frequency $f_0 = 2\tau/(\pi\mu\sigma^2\sigma_n^2)$ (Section 3, Eq. (6)). The spectrally confined terahertz radiation corresponds in time to a multi-cycle electric field with $N$ oscillations within the FWHM. For a slowly varying optical rectification function over $\delta f_{\mathrm{THz}}$, the number of terahertz oscillations is $N = \delta t_n \times f_0 = \delta f_{\mathrm{opt}} \times \tau\sqrt{1 - \sigma^2/\sigma_n^2}$ with $\delta f_{\mathrm{opt}}$ the transform-limited optical pump bandwidth and $\delta t_n$ the FWHM of the chirped optical pulse. The relative terahertz bandwidth is $\delta f_{\mathrm{THz}}/f_0 = \log(2)\sqrt{8}/\pi \times 1/N$ (see Section 3, Eq. (7)). The above relations show that the terahertz central frequency $f_0$, the number of terahertz cycles $N$ and the bandwidth $\delta f_{\mathrm{THz}}$ are easily tunable by adjusting the delay $\tau$ and the chirp rate $\mu$. The details of the theoretical model, which successfully reproduces our experimental results are presented in Section 3. In Section 4 we present broadband and narrowband terahertz generation in OH1. This crystal is well suited for the low-frequency spectral range up to 3 THz. The terahertz field and the spectral intensity are measured with electro-optical sampling (EOS) and a dedicated interferometer. We show that the two diagnostics give comparable results. Finally, terahertz generation, tunable in central frequency and bandwidth up to 7 THz, is obtained in DSTMS organic crystal, as discussed in Section 5.

The terahertz spectral intensity detection was performed using a Michelson-based autocorrelator. Electro-optical sampling (EOS) in (110) gallium phosphide (GaP) of 200 $\mu$m thickness and (110) zinc telluride (ZnTe) of 1 mm thickness was performed for the reconstruction of broadband and narrowband terahertz fields. For the EOS detection, in order to avoid probe polarization over-rotation, we attenuated the pump optical pulse by a factor of 10 and the terahertz by two orders of intensity magnitude. Like this, the resulting electro-optic modulation recorded by EOS is below 10% for transform-limited pump and therefore the detected signal linear with the terahertz electric field. THz low pass filter (LPF8.8-47, Tydex) with cut off frequency at 34 THz is used to filter out the residual pump after the optical rectification. The energy of the terahertz pulse is measured with Golay cell detector (GC-1D, Tydex) and calibrated terahertz attenuators (Tydex). Terahertz beam focus size was measured by the knife-edge method. Terahertz field magnitude was evaluated from the measured energy, pulse duration and focus size as reported in Section 4 and 5.

## 3. Theoretical model

Experimental narrowband terahertz spectra generated in DSTMS [49] and OH1 [50] are simulated by taking into account the characteristics of the organic crystals reported in Refs. [49,50,52,53] such as the velocity matching between the laser pump and the generated terahertz waves as

Optics EXPRESS

well as the optical and terahertz absorption. For the present model we assume a plane-wave and non-depleted pump approximation and neglect cascaded second and higher order nonlinear optical effects. The terahertz generation occurs mainly in the bulk [54]. The contribution of multiple reections in the generation crystals (thickness of 0.4–0.5 mm) is for this analysis neglected. One reason is that the amplitude of the first reflection in the time-domain signal when using transform-limited pump pulses has not been clearly observed, showing that this contribution must be small for this thickness. An estimation based on THz absorption and THz refractive index dispersion shows that for a 0.41 mm thick DSTMS, the first reflection between 1 and 8 THz should contribute less than 0.3% in intensity compared to the main signal. For a 0.45 mm OH1 between 0 and 2 THz, the first reflection is higher and may cause some minor modulation of the spectrum, but it still contributes less than 3% in intensity. For the theoretical considerations in this paper we consider this contribution negligible to keep the analysis simple. The terahertz intensity spectra $I_{\mathrm{THz}}(f)$ are evaluated according to the following formula:

$$I_{\mathrm{THz}}(f) = |t(f) \times T(\lambda) \times H(f,\lambda) \times I_{\mathrm{opt}}(f,\mu,\tau)|^2, \tag{1}$$

where $f = \omega/(2\pi)$ is the terahertz frequency and $\lambda$ denotes the central wavelength of the pump laser. $\mu$ and $\tau$ are the chirp rate and the delay time used to generate the modulated pump pulses, respectively. $t(f)$ and $T(\lambda)$ are the Fresnel transmission coefficients for the terahertz field at the exit surface and for the optical pump at the input face of the crystal, respectively. The optical rectification response function $H(f,\lambda)$ takes into account the velocity matching, the absorption and the second-order nonlinear susceptibility $\chi^{(2)}$ of the organic crystal of thickness $d$ as and is derived from [54] using the above assumptions as:

$$H(f,\lambda) = \frac{\mu_0 \chi^{(2)} \omega^2}{\left(q(f) + q_{\mathrm{opt}}(f,\lambda)\right) n_{\mathrm{opt}}(\lambda) c} \times \frac{e^{iq(f)d} - e^{iq_{\mathrm{opt}}(f,\lambda)d}}{q(f) - q_{\mathrm{opt}}(f,\lambda)} \tag{2}$$

Here $q(f) = \omega/c \times n(f) + i\alpha(f)/2$ is the complex terahertz wave vector ($n(f)$ and $\alpha(f)$ are the refractive index and the absorption coefficient at the terahertz frequency $f$) and $q_{\mathrm{opt}}(f,\lambda) = \omega/c \times n_g(\lambda) + i\alpha_{\mathrm{opt}}(\lambda)$ is the equivalent complex propagation factor for the pump beam envelope ($n_{\mathrm{opt}}(\lambda)$ is the refractive index, $n_g(\lambda)$ the optical group index and $\alpha_{\mathrm{opt}}(\lambda)$ the absorption coefficient at the optical wavelength $\lambda$). The known refractive indices and absorption properties of DSTMS and OH1 [49,50,52,53] at optical and terahertz frequencies are considered in the frequency dependent evaluation of $H(f,\lambda)$ at the employed central laser wavelength of $\lambda = 1230$ nm. A possible terahertz frequency dependence of $\chi^{(2)}$ has not been characterized for these materials yet and is considered negligible here. Note that for our experimental conditions with over 100% photon-conversion efficiency, the non-depleted pump approximation is not valid, therefore the evaluation of the absolute field magnitude is not possible in this approximation. However, we still consider this approximation as a good first approximation to predict the frequency and wavelength dependence of $H(f,\lambda)$ and therefore compare the relative magnitudes of terahertz field components at different frequencies, which is also confirmed experimentally (see e.g. Figure 7(a)). Note also that $H(f,\lambda)$ is very sensitive to the exact velocity matching condition (the denominator in the second factor of Eq. (2)). Since the available optical and terahertz refractive index dispersions [49,50,52,53] have a limited accuracy, the resulting frequency dependence may deviate in details from the experimental one (compare the black curves in Figs. 6(b) and 6(d)), however, the overall spectral features such as the position of spectral gaps are predicted reasonably well.

$I_{\mathrm{opt}}(f,\mu,\tau)$ in Eq. (1) is the Fourier transformation of the modulated pump intensity $I_{\mathrm{opt}}(t,\mu,\tau)$. For the modulated pump beam, we consider the interference pattern of two linearly chirped pulses of the form

$$E(t) = \frac{1}{2} E_0 \times \sqrt{\sigma/\sigma_n} \times \exp\left(-i\omega_0 t\right) \times \exp\left(-\frac{t^2}{\sigma_n^2}\left(1 - i\frac{2}{\mu\sigma^2}\right)\right) \tag{3}$$

Optics EXPRESS

delayed in time by $\tau$. Here $\sigma = \delta t/\sqrt{2\log(2)}$ and $\sigma_n = \delta t_n/\sqrt{2\log(2)}$ represent the $e^{-1}$ half-width of the transform-limited and the chirped fields, respectively, where $\delta t$ and $\delta t_n$ denote the corresponding FWHM duration of the pulse intensities. For a given chirp rate $\mu$, the pulse duration is $\sigma_n = \sigma \times \sqrt{1 + (2/\mu\sigma^2)^2}$ [55]. The intensity of the combined pulses is then given by [55]

$$I_{\mathrm{opt}}(t, \mu, \tau) = |E(t + \tau/2) + E(t - \tau/2)|^2 = I_+(t) + I_-(t) + I_{\mathrm{cross}}(t) \tag{4}$$

where $I_\pm = E_0^2(\sigma/4\sigma_n)\exp(-2(t \pm \tau/2)^2/\sigma_n^2)$ are the intensities of the individual chirped pulses and the cross term expresses the interference

$$I_{\mathrm{cross}}(t) = E_0^2 \times \frac{\sigma}{2\sigma_n} \times \exp(-\tau^2/2\sigma_n^2) \times \exp(-2t^2/\sigma_n^2) \times \cos\left(\omega_0\tau + \frac{4\tau}{\mu\sigma^2\sigma_n^2}t\right). \tag{5}$$

Note that the expression 5 simplifies to the one given in [55] for $\sigma_n \gg \sigma(\delta t_n \gg \delta t)$. The cross term oscillates with the beating frequency of

$$f_0 = \frac{2\tau}{\pi\mu\sigma^2\sigma_n^2} \left(\text{or } f_0 \cong \frac{2\log(2)\tau}{\pi\delta t\delta t_n} \text{ for } \delta t_n \gg \delta t\right). \tag{6}$$

The beating frequency of the pump determines the central frequency of the emitted terahertz radiation and is proportional to the ratio between the delay time $\tau$ and the duration of the chirped pulses $\delta t_n$ for a given duration of the transform-limited pulses $\delta t$.

The number of cycles $N$ within the FWHM of the optical intensity envelope can be evaluated from $I_{\mathrm{cross}}(t)$ according to $N = \delta t_n \times f_0 = \delta f_{\mathrm{opt}} \times \tau\sqrt{(1 - \delta t^2/\delta t_n^2)}$, which reduces to $N = \delta f_{\mathrm{opt}}\tau$ in case of large chirp $\delta t_n \gg \delta t$. Here $\delta f_{\mathrm{opt}}$ is the spectral bandwidth of the transform-limited pump pulses with the time-bandwidth product of $\delta f_{\mathrm{opt}} \cdot \delta t = 2\log(2)/\pi$. The number of cycles is therefore mainly determined by the delay time $\tau$ [40].

The FWHM bandwidth of the intensity modulation $|I_{\mathrm{opt}}(f, \mu, \tau)|^2$ at the central frequency $f_0$ is evaluated as $\delta f_{\mathrm{THz}} = \log(2)\sqrt{8}/(\pi\delta t_n)$ and is therefore fully defined by the FWHM duration of the chirped pulse $\delta t_n$. This will be approximately equal to the bandwidth of the final terahertz intensity spectrum, in case the material response function $H(f, \lambda)$ differs slightly within this bandwidth. The ratio between the bandwidth and the central frequency of the obtained terahertz pulse scales with the number of pulses $N$ within the FWHM of the intensity modulation as

$$\frac{\delta f_{\mathrm{THz}}}{f_0} = \frac{\log(2)\sqrt{8}}{\pi} \times \frac{1}{N} \approx \frac{\log(2)\sqrt{8}}{\pi\delta f_{\mathrm{opt}}} \times \frac{1}{\tau} \tag{7}$$

which is valid for small variations of $H(f, \lambda)$ within the bandwidth. Note that the above expressions are valid in case of linear chirp only; in case of an additional quadratic chirp, the bandwidth $\delta f_{\mathrm{THz}}$ will additionally increase [55].

## 4. Broadband and narrowband terahertz generation in OH1

The largest terahertz spectral output is achieved using un-chirped pump pulses. In this configuration and without frequency beating, the temporal shape of the pump pulse is approximately Gaussian with a FWHM pulse duration of $\delta t$ = 120 fs. The resulting single-cycle terahertz pulse produced by OR in OH1 and the spectral intensity are reconstructed by multi-shot EOS in gallium phosphide (GaP) crystal. The terahertz electric field is an asymmetric single cycle pulse with peak strength of 22.4 MV/cm (Fig. 2(a)) and carries the main part of spectral components ranging from 0.1 to 3 THz with centroid frequency at 1.55 THz (Fig. 2(b)).

At a fluence of 15 mJ/cm$^2$ and pump energy of 10 mJ, the optical rectification process in OH1 (12 mm in diameter, from Rainbow Photonics AG) yields to terahertz output energy of $\varepsilon_{\mathrm{THz}}$ = 280 $\mu$J, corresponding to an energy conversion efficiency of 2.8% (terahertz pulse energy

Optics EXPRESS

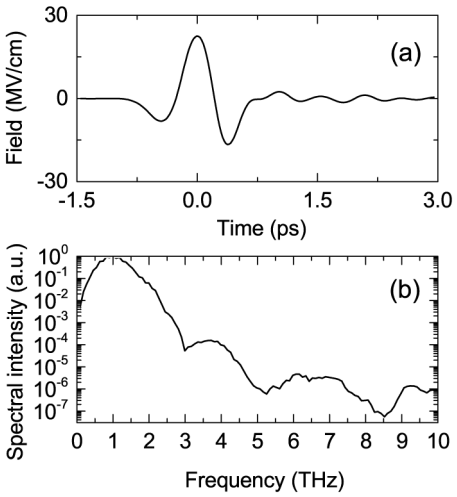


**Fig. 2.** Broadband terahertz radiation. (a) Optical rectification of the transform-limited pump pulse in the organic crystal OH1 gives rise to a single-cycle terahertz field carrying a broad spectrum between 0.1 and 3 THz. (b) The field shape and spectral intensity are reconstructed in free-space electro-optical sampling carried out in a 200-μm thick GaP crystal.

divided by the pump laser energy). This corresponds to a photon conversion efficiency of 439% (number of terahertz photons per incident laser photons in percent), which indicates a cascaded optical rectification process [20]. For the smaller-area organic crystal DSTMS, pumped by 4.3 mJ, similar energy conversion efficiency (2.9%) is achieved, with an output energy of $\varepsilon_{\mathrm{THz}}$ = 125 $\mu$J at slightly lower photon efficiency (307%). The corresponding peak field strength of 24 MV/cm is calculated from the measured terahertz pulse energy (125 $\mu$J), THz pulse duration $\tau_{\mathrm{THz}}$ (0.435 ps FWHM) and diffraction-limited beam diameter (125 $\mu$m, FWHM). The assumption of diffraction-limited properties for the present single-cycle THz source is consistent with previous results, where the focus size was limited only by not perfect focusing system [51]. The peak field is determined according to the formula $E_{\mathrm{THz}} = \sqrt{\varepsilon_{\mathrm{THz}}/\left(c\epsilon_0\tau_{\mathrm{THz}}\pi r^2\right)}$ being c the speed of light, $\varepsilon_{\mathrm{THz}}$ the terahertz pulse energy, $2r$ the spot size diameter (at 1/e level) and $\epsilon_0$ the electric permittivity of free space. The peak field is in agreement with previous results, considering a non-optimized focusing system used there [51]. Although the Cr:Forsterite laser system is not carrier-envelope phase-stabilized, the terahertz pulses are phase-locked and carry an absolute phase, which is constant for consecutive shots as demonstrated by the multi-shot field reconstruction using EOS. This is expected from the optical rectification process where, owing to difference frequency generation between two intrapulse spectral components, the common phase offset is removed.

The modulated laser intensity obtained with two 4 ps chirped pulses and delay of 1.5 ps is converted to ten cycles terahertz field in an organic crystal OH1 (Fig. 3).

The temporal and spectral characteristics are retrieved using electro-optical sampling and first order autocorrelation based on Michelson interferometer. The first diagnostic permits complete reconstruction of the terahertz field. However, multiple reflections at the 0.2-mm-thick GaP crystal surfaces limit the scanning temporal window, and ultimately the spectral resolution. To avoid this effect, 1-mm-thick ZnTe crystal was used; however such thick electro-optical medium presents sufficient spectral sensitivity only at low terahertz frequencies (< 2 THz) and is characterized by a lower signal-to-noise ratio. The field autocorrelation is a viable alternative

Optics EXPRESS

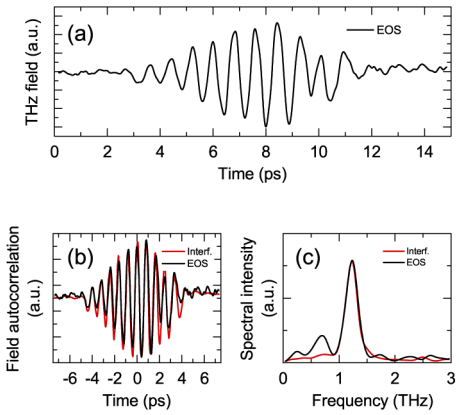


**Fig. 3.** Narrowband/multicycle terahertz radiation. (a) Optical rectification by two chirped and delayed pump pulses (chirped pulse duration $\delta\tau_n = 4$ ps, delay time $\tau = 1.5$ ps) in the organic crystal OH1 gives rise to a multi-cycle terahertz field measured by EOS. (b), (c) The field autocorrelation and the narrowband spectral intensity are reconstructed using either EOS from (a) (black) or measured by field autocorrelation in a Michelson interferometer (red). The temporal and spectral terahertz characteristics obtained by EOS and by first order autocorrelation are in a good agreement.

diagnostic for tunable narrowband terahertz spectra. As shown in Figs. 3(b) and 3(c), the field autocorrelation and the spectral intensity reconstructed with the terahertz interferometer are comparable to the results obtained with the electro-optical sampling.

In order to gain control over the spectral width and the central frequency of the terahertz output, the shape of the pump pulse is properly modified by chirping and delaying two pump replicas.

Narrowband terahertz radiation in the low frequency terahertz part (0.1–1.5 THz) is of particular interest in quantum physics to selectively excite low-energy states with narrow linewidths. In order to provide a spectrally confined tunable source in this frequency range, we optimized the generation conditions by employing an OH1 organic crystal [56]. While terahertz emission from DSTMS is affected by a strongly absorbing phonon resonance at 1 THz, the OH1 crystal emits broadband radiation centred at 1 THz when pumped with a transform-limited pulse from Cr:Fosterite laser (Fig. 2(b)). Figure 4 shows the continuous tuning range of the OH1 source over almost three octaves when pumped with our modulated pump configuration. The central frequencies $f_0$ between 0.28 and 1.7 THz are achieved by modifying the delay between two chirped pulses of the laser pump accordingly, Fig. 4(a).

The minimum measured bandwidth of 30 GHz is sufficiently narrow to selectively drive a quantum state with a table-top terahertz source. The energy conversion efficiency across the frequency conversion range provided by OH1 is $\approx 0.02\%$ and reaches up to 4.7 $\mu$J (central frequency at 1.1 THz) in our experiment. The narrowband spectral position, the bandwidth and relative intensities are reproduced well by the theoretical model employed. The corresponding peak electric field strength is of several MV/cm at the diffraction limited focus. This strength is almost two orders of magnitude beyond the state of the art of laser-based sources and comparable to what is achieved at large-size T-FEL facilities. In principle, even narrower bandwidth could be achieved with our scheme by employing a pump beam with a super-Gaussian-like temporal shape by means of an infrared spectral shaper. However, such a shaper was not available for this proof-of-principle study.

Diffraction-limited focus size was already experimentally verified for broadband sources using the same Cr:forsterite laser pump and various organic crystals [51]. It is expected that if a broadband spectrum can be focused to the physical limit, also a narrowband part of the

Optics EXPRESS

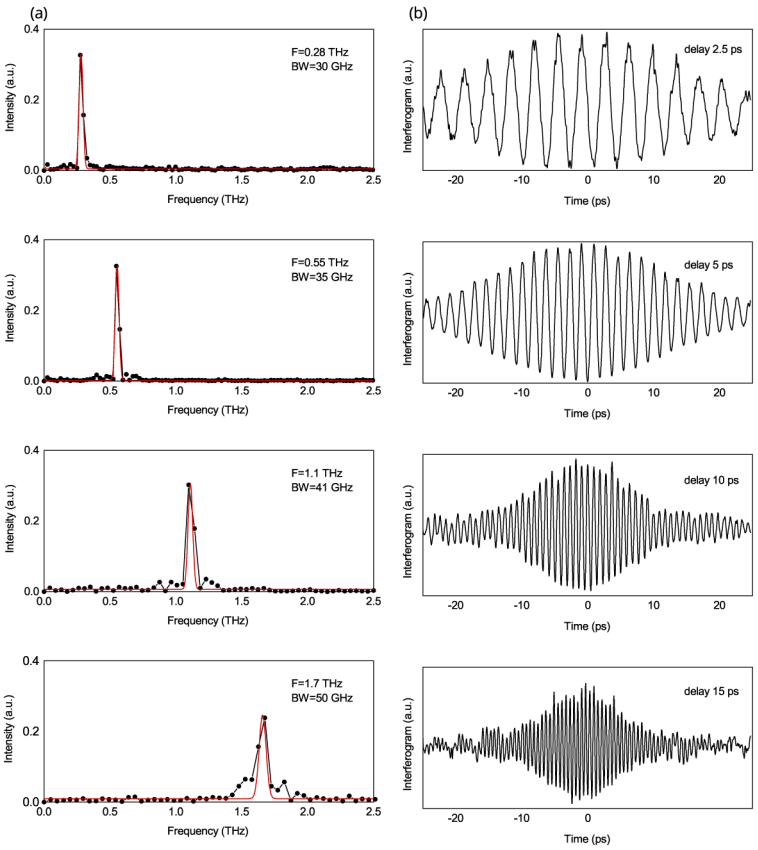


**Fig. 4.** (a) Narrowband terahertz radiation continuously tunable across the 3-octave spanning low terahertz frequency range (0.2–1.6 THz) by employing chirp-and-delay pulses for OR in the organic crystal OH1. The experimental spectral intensity (black points) is well reproduced by numerical simulated spectral intensity (red curve). (b) The corresponding pump beating pattern is shown as well. The chirped pulse duration was 30 ps (FWHM) and time delays between two chirped pulses were 2.5 ps, 5 ps, 10 ps and 15 ps.

spectrum can be focused to the diffraction-limited spot size. In order to support this assumption, the focus size of different narrowband terahertz pulses generated in the OH1 crystal having a 4-mm emission diameter and focused with an F-number of #F=5/4 was measured. The diffraction-limited diameter at half maximum (FWHM) of Gaussian beam is calculated by formula: $D_{\mathrm{FWHM}} = 0.75\lambda_{\mathrm{THz}}\#F$, where $\lambda_{\mathrm{THz}}$ is the THz wavelength. We remind that OH1 generates mainly low frequency radiation up to 3 THz, therefore we limit the measurement of the focus to narrowband radiation between 1 and 2 THz. The focus size is experimentally reconstructed by standard knife-edge technique. The beam intensity distribution $I_{\mathrm{THz}}(x)$ is simply retrieved by derivative of the THz power not intercepted by the blade. As THz power detector, a Golay cell is used. The measurements are performed at different positions along the beam propagation to find the longitudinal coordinate of the waist. The blade is moved with steps of 50 $\mu$m or 100 $\mu$m and for each knife-edge scan at least 20 blade positions are recorded. The shot-to-shot laser fluctuations (>5% rms) are partially suppressed by averaging.

The narrowband radiation for this measurement is produced in the setup of Fig. 1 with chirped pulse duration of 2 ps and delay time of 0.7, 1 and 1.5 ps, respectively.

Optics EXPRESS

The spectral intensities (left plots of Fig. 5) are reconstructed by first order interferometry, and present a constant bandwidth of about 370 GHz at central frequency of 1, 1.45 and 2 THz. The repeatability of the scans was not extensively studied, however for two successive measurements give results within 10%. The intensity profile $I_{\mathrm{THz}}(x)$ is calculated by derivative of the knife-edge scans. The Gaussian function

$$I_{\mathrm{THz}}(x) = I_0 \exp\left(-0.5\left(\frac{x - x_c}{s}\right)^2\right)$$

approximates quite well $I_{\mathrm{THz}}(x)$ and is used to determine the diameter of beam at half maximum ($D_{\mathrm{FWHM}} = 2s\sqrt{\ln(4)}$). For the measured configuration, the calculated limit of diffraction and the measured $D_{\mathrm{FWHM}}$ are reported in Table 1. The focus sizes are close to the diffraction-limited ones. The small discrepancies can be explained either by laser energy drift over the scan time and the uncertainly in the central frequency.

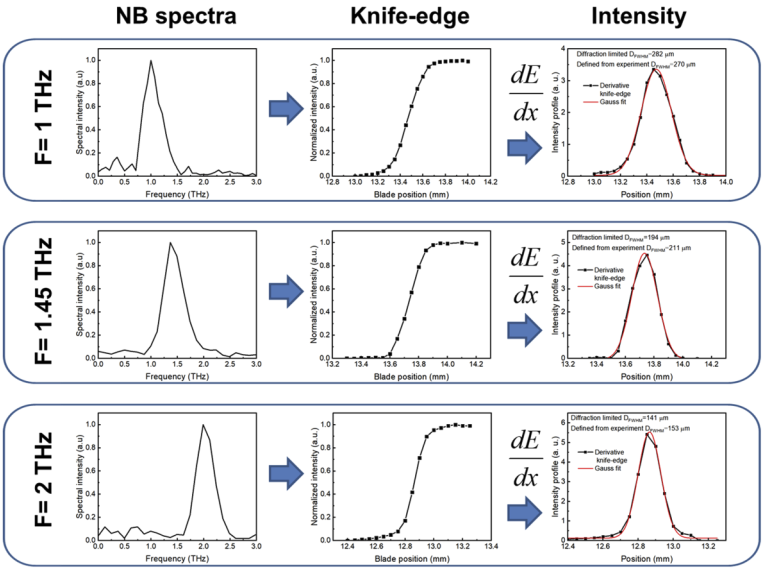


**Fig. 5.** From left to right: spectral intensity, knife-edge power measurement and transverse intensity profile. From top to bottom: narrowband radiation at 1, 1.45 and 2 THz. The transverse intensity profile is fitted with a Gaussian function (red curve) to calculate the FWHM.

**Table 1. The measured focal spot diameters and the calculated diffraction-limited spot diameters**

| Frequency | #F-number | Knife-edge $D_{\mathrm{FWHM}}$, $\mu$m | Diffraction-limited $D_{\mathrm{FWHM}}$, $\mu$m |
|---|---|---|---|
| 1 THz | 1 | 270 | 282 |
| 1.45 THz | 1.2 | 211 | 194 |
| 2 THz | 1.2 | 153 | 141 |

## 5. Highly tunable narrowband terahertz generation in DSTMS

The broadband phase-matching range of the organic crystals DSTMS (thickness of 410 $\mu$m and diameter of 7 mm, from Rainbow Photonics AG) allows for a continuous tunability of the center frequency between 0.5 and 7 THz, which is demonstrated in Fig. 6(a).

Optics EXPRESS

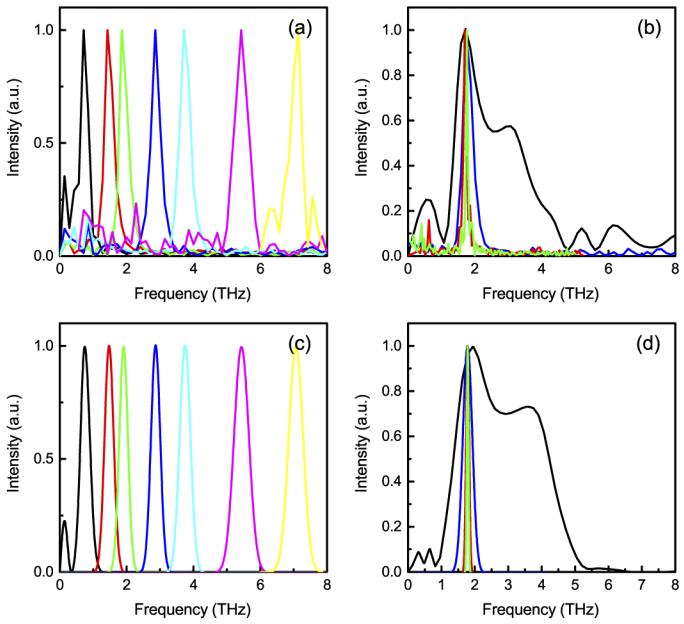


**Fig. 6.** Frequency and bandwidth tunability of strong-field terahertz pulses across the terahertz gap. The spectra are displayed by different colours. (a) The scheme based on Cr:Forsterite pumped organic crystals provides an extreme coverage over almost 4 octaves, from 0.5 to 7 THz. The chirped pulse duration was 1.9 ps (FWHM) and time delays between two chirped pulses were 300 fs, 700 fs, 1 ps, 1.5 ps, 2 ps, 3 ps and 4 ps. (b) The naturally broadband terahertz spectrum (black curve) from the transform limited pump pulse is adjusted by employing frequency beating and chirp of the pump pulse (blue — delay was 1 ps, duration was 1.9 ps, red — delay was 4.5 ps, duration was 8.5 ps, green — delay was 8.5 ps, duration was 17 ps). The bandwidth can be continuously reduced from several octaves to <50 GHz (FWHM). In (c) and (d) the corresponding theoretical spectra are shown.

The resulting narrowband, multicycle terahertz pulses are generated with a chirp-and-delay setting specific to each central frequency in order to keep the relative bandwidth constant at ≈15% across the demonstrated tuning range. Our scheme gives a straight-forward control on the spectral bandwidth by chirp and delay adjustment of the pump pulses. Figure 6(b) shows the evolution of the bandwidth when the chirped pulses are broadened from transform-limited 120 fs to 20 ps. The spectrum is continuously reduced and results finally in a 45 GHz FWHM spectral line (green) at 1.8 THz, corresponding to a relative bandwidth of 2.5%. For this set of measurements, the ratio between the delay time and the chirped pulse duration is kept constant in order to keep the resulting spectrum centred at the targeted 1.8 THz. In general, spectrally narrowband radiation with a linewidth down to a few percent can be produced over the crystal optical rectification bandwidth. The terahertz central frequency and bandwidth of the tuning experiment can be accurately reproduced by our theoretical model, as shown in Figs. 6(c) and 6(d).

Figure 7 shows the pulse energy and the average and peak electric field for the different spectra presented in Fig. 6(a). The average field of the oscillation is given by the peak field $E_{\mathrm{THz}}$ divided by $\sqrt{2}$, which could be a more appropriate quantity to determine the effective resonant excitation with multicycle THz pulses.

The narrowband terahertz beam at different frequencies should be focused close to the diffraction limit for the realization of the highest field. Diffraction-limited property of broadband

Optics EXPRESS

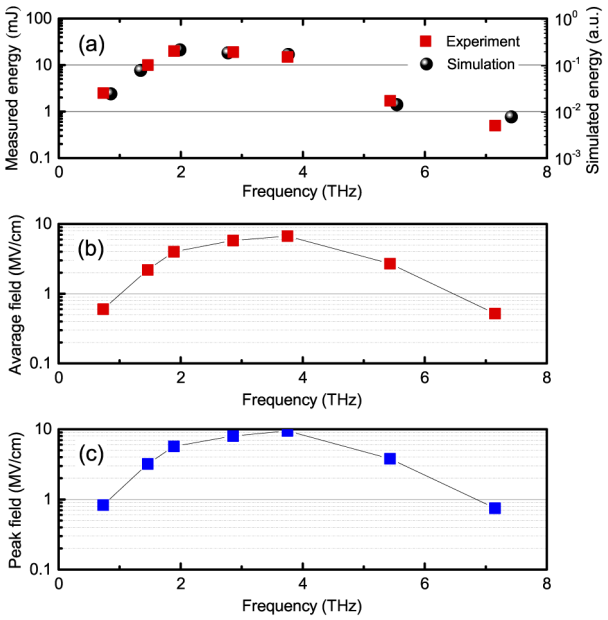


**Fig. 7.** (a) THz pulse energy, (b) average electric field strength and (c) peak field strength of these narrowband pulses. The relative terahertz pulse energies measured in the experiment are well approximated by the theoretical model. The field strength is calculated from the terahertz pulse energy, the terahertz pulse duration and the minimum possible size at the diffraction-limited focus. The terahertz pulse duration for all the central wavelengths is retrieved by the first order autocorrelation measurements.

radiation [13] extends also for narrowband THz radiation. In fact, if a broadband radiation can be focused to the physical limit, also part of its spectrum can, as in the case of narrowband radiation. The diffraction-limited beam properties have been verified for narrowband THz radiation produced in OH1 using the knife edge technique as described in Section 4, which complements earlier measurements on a broadband THz radiation from OH1 and DSTMS [13]. The terahertz pulse energy can reach 20 $\mu$J for frequencies around 2–3 THz where the transform limited spectrum shows the largest spectral density (Fig. 6(b)). The corresponding energy conversion efficiency of 0.27% (7.5 mJ pump, 20 $\mu$J THz output) is more than an order of magnitude higher than what has been reported in the past for laser-based narrowband terahertz sources [40,42]. The relative pulse energies at different central frequencies match with the theoretical model well. As expected, the optical rectification efficiency in the organic crystal is frequency-dependent and the terahertz pulse energy for narrowband pulses scales in frequency according to the spectral intensity versus frequency obtained by a transform-limited pump pulse. The energy carried by a narrowband terahertz pulse, Fig. 6(c), is observed to scale in first order with the FWHM spectral bandwidth. The largest peak electric field of 8 MV/cm is achieved at around the 4 THz centre frequency and reduces towards the edges due to the phase-matching issues and due to the transform-limited pulse duration (higher frequency range) and frequency-dependent increase of the diffraction-limited focus size (lower frequency range).

Finally, our scheme allows for a variety of intrinsically jitter-free multicolor pump and optical probe schemes while offering terahertz pulse shaping capabilities covering single-cycle, at tens of MV/cm field, as well as many-cycle pulses with several MV/cm field strength. Scaling towards larger field strength and pulse energy and subsequently larger field strength is straightforward by

Optics EXPRESS

employing higher pump energy and larger-area organic crystals, while keeping the pump fluence below the laser-induced damage threshold (<20 mJ/cm$^2$).

## 6. Conclusion

In conclusion, we demonstrated a versatile high-peak power terahertz source capable of delivering both a broadband spectrum as well as narrowband terahertz radiation, continuously tunable in central frequency and bandwidth between 0.5 and 7 THz. The pump-pulse intensity profile modulated by frequency beating of two chirped pulse replicas is optically rectified in the highly efficient organic crystal DSTMS and OH1. We employed a unique Cr:Forsterite chirped-pulse amplification laser proving very high pulse energies up to 20 mJ at 120 fs pulse duration, which combined with the high second-order optical nonlinearity of DSTMS and OH1 crystals and their good phase matching between the Cr:Forsterite wavelength and the target THz frequency range allows for generating very intense THz waves. The terahertz output linewidth is tunable across a frequency range of 0.03–5 THz and offers a record small bandwidth of 30 GHz. When pumped with 10 mJ, the highly efficient organic-crystal-based terahertz generation provides up to 280 $\mu$J broadband THz pulse energy and 4.7 $\mu$J in a 41-GHz narrowband mode at 1.1 THz, at an energy conversion efficiency of 2.8% and 0.05%, respectively. We present a theoretical model of narrowband and broadband terahertz generation in organic crystals, which reproduced the experimental results with excellent accuracy.

The unprecedented field strength of tens of MV/cm (single-cycle) and several of MV/cm (multi-cycle) opens new scientific pathways for selective and nonlinear excitation of low-energy modes in condensed matter. Moreover, the presented source opens new prospective for the realization of compact electron accelerators [57] and for advanced imaging applications.

## Funding

Schweizerischer Nationalfonds zur Förderung der Wissenschaftlichen Forschung (IZKSZ2_162129, IZLRZ2_164051); Russian Foundation for Basic Research (20-08-00627, 20-21-00043).

## Acknowledgment

The experiments were performed using the unique scientific facility "Terawatt Femtosecond Laser Complex" in the "Femtosecond Laser Complex" Center of the Joint Institute for High Temperatures of the Russian Academy of Sciences. The reported study was funded by RFBR, project number 20-08-00627, and by RFBR and ROSATOM, project number 20-21-00043.

## Disclosures

The authors declare no conflicts of interest.

## References

1. I. Katayama, H. Aoki, J. Takeda, H. Shimosato, M. Ashida, R. Kinjo, I. Kawayama, M. Tonouchi, M. Nagai, and K. Tanaka, "Ferroelectric soft mode in a SrTiO3 thin film impulsively driven to the anharmonic regime using intense picosecond terahertz pulses," Phys. Rev. Lett. **108**(9), 097401 (2012).
2. T. Kampfrath, A. Sell, G. Klatt, A. Pashkin, S. Mährlein, T. Dekorsy, M. Wolf, M. Fiebig, A. Leitenstorfer, and R. Huber, "Coherent terahertz control of antiferromagnetic spin waves," Nat. Photonics **5**(1), 31–34 (2011).
3. F. Chen, Y. Zhu, S. Liu, Y. Qi, H. Y. Hwang, N. C. Brandt, J. Lu, F. Quirin, H. Enquist, P. Zalden, T. Hu, J. Goodfellow, M.-J. Sher, M. C. Hoffmann, D. Zhu, H. Lemke, J. Glownia, M. Chollet, A. R. Damodaran, J. Park, Z. Cai, I. W. Jung, M. J. Highland, D. A. Walko, J. W. Freeland, P. G. Evans, A. Vailionis, J. Larsson, K. A. Nelson, A. M. Rappe, K. Sokolowski-Tinten, L. W. Martin, H. Wen, and A. M. Lindenberg, "Ultrafast terahertz-field-driven ionic response in ferroelectric BaTiO3," Phys. Rev. B **94**(18), 180104 (2016).
4. K. A. Grishunin, N. A. Ilyin, N. E. Sherstyuk, E. D. Mishina, A. Kimel, V. M. Mukhortov, A. V. Ovchinnikov, O. V. Chefonov, and M. B. Agranat, "THz electric field-induced second harmonic generation in inorganic ferroelectric," Sci. Rep. **7**(1), 687 (2017).

Optics EXPRESS


5. M. C. Beard, G. M. Turner, and C. A. Schmuttenmaer, "Terahertz spectroscopy," J. Phys. Chem. B **106**(29), 7146–7159 (2002).
6. M. Tonouchi, "Cutting-edge terahertz technology," Nat. Photonics **1**(2), 97–105 (2007).
7. R. Ulbricht, E. Hendry, J. Shan, T. F. Heinz, and M. Bonn, "Carrier dynamics in semiconductors studied with time-resolved terahertz spectroscopy," Rev. Mod. Phys. **83**(2), 543–586 (2011).
8. T. Arikawa, X. Wang, D. J. Hilton, J. L. Reno, W. Pan, and J. Kono, "Quantum control of a landau-quantized two-dimensional electron gas in a GaAs quantum well using coherent terahertz pulses," Phys. Rev. B **84**(24), 241307 (2011).
9. M. Wagner, H. Schneider, D. Stehr, S. Winnerl, A. M. Andrews, S. Schartner, G. Strasser, and M. Helm, "Observation of the intraexciton autler-townes effect inGaAs/AlGaAsSemiconductor quantum wells," Phys. Rev. Lett. **105**(16), 167401 (2010).
10. S. Kovalev, Z. Wang, J.-C. Deinert, N. Awari, M. Chen, B. Green, S. Germanskiy, T. V. A. G. de Oliveira, J. S. Lee, A. Deac, D. Turchinovich, N. Stojanovic, S. Eisebitt, I. Radu, S. Bonetti, T. Kampfrath, and M. Gensch, "Selective THz control of magnetic order: new opportunities from superradiant undulator sources," J. Phys. D: Appl. Phys. **51**(11), 114007 (2018).
11. S. Maehrlein, A. Paarmann, M. Wolf, and T. Kampfrath, "Terahertz sum-frequency excitation of a raman-active phonon," Phys. Rev. Lett. **119**(12), 127402 (2017).
12. M. Kozina, M. Fechner, P. Marsik, T. van Driel, J. M. Glownia, C. Bernhard, M. Radovic, D. Zhu, S. Bonetti, U. Staub, and M. C. Hoffmann, "Terahertz-driven phonon upconversion in SrTiO3," Nat. Phys. **15**(4), 387–392 (2019).
13. M. Shalaby and C. P. Hauri, "Demonstration of a low-frequency three-dimensional terahertz bullet with extreme brightness," Nat. Commun. **6**(1), 5976 (2015).
14. C. Vicario, C. Ruchert, F. Ardana-Lamas, P. M. Derlet, B. Tudu, J. Luning, and C. P. Hauri, "Off-resonant magnetization dynamics phase-locked to an intense phase-stable terahertz transient," Nat. Photonics **7**(9), 720–723 (2013).
15. T. Kampfrath, K. Tanaka, and K. A. Nelson, "Resonant and nonresonant control over matter and light by intense terahertz transients," Nat. Photonics **7**(9), 680–690 (2013).
16. E. Mashkovich, K. Grishunin, R. Mikhaylovskiy, A. Zvezdin, R. Pisarev, M. Strugatsky, P. Christianen, T. Rasing, and A. Kimel, "Terahertz optomagnetism: Nonlinear THz excitation of GHz spin waves in antiferromagnetic FeBO3," Phys. Rev. Lett. **123**(15), 157202 (2019).
17. H. Hirori, A. Doi, F. Blanchard, and K. Tanaka, "Single-cycle terahertz pulses with amplitudes exceeding 1 MV/cm generated by optical rectification in LiNbO3," Appl. Phys. Lett. **98**(9), 091106 (2011).
18. J. A. Fülöp, Z. Ollmann, C. Lombosi, C. Skrobol, S. Klingebiel, L. Pálfalvi, F. Krausz, S. Karsch, and J. Hebling, "Efficient generation of THz pulses with 04 mJ energy," Opt. Express **22**(17), 20155–20163 (2014).
19. X. jun Wu, J. long Ma, B. long Zhang, S. su Chai, Z. ji Fang, C.-Y. Xia, D. yin Kong, J. guang Wang, H. Liu, C.-Q. Zhu, X. Wang, C.-J. Ruan, and Y.-T. Li, "Highly efficient generation of 02 mJ terahertz pulses in lithium niobate at room temperature with sub-50 fs chirped ti:sapphire laser pulses," Opt. Express **26**(6), 7107 (2018).
20. C. Vicario, B. Monoszlai, and C. P. Hauri, "GV/mSingle-cycle terahertz fields from a laser-driven large-size partitioned organic crystal," Phys. Rev. Lett. **112**(21), 213901 (2014).
21. M. Clerici, M. Peccianti, B. E. Schmidt, L. Caspani, M. Shalaby, M. Giguère, A. Lotti, A. Couairon, F. Légaré, T. Ozaki, D. Faccio, and R. Morandotti, "Wavelength scaling of terahertz generation by gas ionization," Phys. Rev. Lett. **110**(25), 253901 (2013).
22. P. G. de Alaiza Martínez, I. Babushkin, L. Bergé, S. Skupin, E. Cabrera-Granado, C. Köhler, U. Morgner, A. Husakou, and J. Herrmann, "Boosting terahertz generation in laser-field ionized gases using a sawtooth wave shape," Phys. Rev. Lett. **114**(18), 183901 (2015).
23. P. G. de Alaiza Martínez, X. Davoine, A. Debayle, L. Gremillet, and L. Bergé, "Terahertz radiation driven by two-color laser pulses at near-relativistic intensities: Competition between photoionization and wakefield effects," Sci. Rep. **6**(1), 26743 (2016).
24. V. Y. Fedorov and S. Tzortzakis, "Extreme THz fields from two-color filamentation of midinfrared laser pulses," Phys. Rev. A **97**(6), 063842 (2018).
25. S. Casalbuoni, B. Schmidt, P. Schmüser, V. Arsov, and S. Wesch, "Ultrabroadband terahertz source and beamline based on coherent transition radiation," Phys. Rev. Spec. Top.–Accel. Beams **12**(3), 030705 (2009).
26. Z. Wu, A. S. Fisher, J. Goodfellow, M. Fuchs, D. Daranciang, M. Hogan, H. Loos, and A. Lindenberg, "Intense terahertz pulses from SLAC electron beams using coherent transition radiation," Rev. Sci. Instrum. **84**(2), 022701 (2013).
27. E. Chiadroni, A. Bacci, M. Bellaveglia, M. Boscolo, M. Castellano, L. Cultrera, G. D. Pirro, M. Ferrario, L. Ficcadenti, D. Filippetto, G. Gatti, E. Pace, A. R. Rossi, C. Vaccarezza, L. Catani, A. Cianchi, B. Marchetti, A. Mostacci, L. Palumbo, C. Ronsivalle, A. D. Gaspare, M. Ortolani, A. Perucchi, P. Calvani, O. Limaj, D. Nicoletti, and S. Lupi, "The SPARC linear accelerator based terahertz source," Appl. Phys. Lett. **102**(9), 094101 (2013).
28. P. Tan, J. Huang, K. Liu, Y. Xiong, and M. Fan, "Terahertz radiation sources based on free electron lasers and their applications," Sci. China Inf. Sci. **55**(1), 1–15 (2012).
29. Y. Shen, X. Yang, G. L. Carr, Y. Hidaka, J. B. Murphy, and X. Wang, "Tunable few-cycle and multicycle coherent terahertz radiation from relativistic electrons," Phys. Rev. Lett. **107**(20), 204801 (2011).

Optics EXPRESS


30. B. Green, S. Kovalev, V. Asgekar, G. Geloni, U. Lehnert, T. Golz, M. Kuntzsch, C. Bauer, J. Hauser, J. Voigtlaender, B. Wustmann, I. Koesterke, M. Schwarz, M. Freitag, A. Arnold, J. Teichert, M. Justus, W. Seidel, C. Ilgner, N. Awari, D. Nicoletti, S. Kaiser, Y. Laplace, S. Rajasekaran, L. Zhang, S. Winnerl, H. Schneider, G. Schay, I. Lorincz, A. A. Rauscher, I. Radu, S. Mährlein, T. H. Kim, J. S. Lee, T. Kampfrath, S. Wall, J. Heberle, A. Malnasi-Csizmadia, A. Steiger, A. S. Müller, M. Helm, U. Schramm, T. Cowan, P. Michel, A. Cavalleri, A. S. Fisher, N. Stojanovic, and M. Gensch, "High-field high-repetition-rate sources for the coherent THz control of matter," Sci. Rep. **6**(1), 22256 (2016).
31. "FELIX laboratory http://www.ru.nl/felix/,".
32. C. Wang, W. Xu, H.-Y. Mei, H. Qin, X.-N. Zhao, H. Wen, C. Zhang, L. Ding, Y. Xu, P. Li, D. Wu, and M. Li, "Picosecond terahertz pump-probe realized from Chinese terahertz free-electron laser," Chin. Phys. B **29**(8), 084101 (2020).
33. F. Wang, J. Lee, D. J. Phillips, S. G. Holliday, S.-L. Chua, J. Bravo-Abad, J. D. Joannopoulos, M. Soljačić, S. G. Johnson, and H. O. Everitt, "A high-efficiency regime for gas-phase terahertz lasers," Proc. Natl. Acad. Sci. **115**(26), 6614–6619 (2018).
34. M. C. Hoffmann and J. A. Fülöp, "Intense ultrashort terahertz pulses: generation and applications," J. Phys. D: Appl. Phys. **44**(8), 083001 (2011).
35. M. Jazbinsek, U. Puc, A. Abina, and A. Zidansek, "Organic crystals for THz photonics," Appl. Sci. **9**(5), 882 (2019).
36. A. G. Stepanov, J. Hebling, and J. Kuhl, "Generation, tuning, and shaping of narrow-band, picosecond THz pulses by two-beam excitation," Opt. Express **12**(19), 4650 (2004).
37. S. Vidal, J. Degert, J. Oberlé, and E. Freysz, "Femtosecond optical pulse shaping for tunable terahertz pulse generation," J. Opt. Soc. Am. B **27**(5), 1044–1050 (2010).
38. K. L. Vodopyanov, "Optical generation of narrow-band terahertz packets in periodically-inverted electro-optic crystals: conversion efficiency and optimal laser pulse format," Opt. Express **14**(6), 2263–2276 (2006).
39. A. S. Weling, B. B. Hu, N. M. Froberg, and D. H. Auston, "Generation of tunable narrow-band THz radiation from large aperture photoconducting antennas," Appl. Phys. Lett. **64**(2), 137–139 (1994).
40. Z. Chen, X. Zhou, C. A. Werley, and K. A. Nelson, "Generation of high power tunable multicycle teraherz pulses," Appl. Phys. Lett. **99**(7), 071102 (2011).
41. J. Lu, H. Y. Hwang, X. Li, S.-H. Lee, O.-P. Kwon, and K. A. Nelson, "Tunable multi-cycle THz generation in organic crystal HMQ-TMS," Opt. Express **23**(17), 22723–22729 (2015).
42. B. Liu, H. Bromberger, A. Cartella, T. Gebert, M. Först, and A. Cavalleri, "Generation of narrowband, high-intensity, carrier-envelope phase-stable pulses tunable between 4 and 18 THz," Opt. Lett. **42**(1), 129–131 (2017).
43. K. Ravi, D. N. Schimpf, and F. X. Kärtner, "Pulse sequences for efficient multi-cycle terahertz generation in periodically poled lithium niobate," Opt. Express **24**(22), 25582–25607 (2016).
44. S. W. Jolly, N. H. Matlis, F. Ahr, V. Leroux, T. Eichner, A.-L. Calendron, H. Ishizuki, T. Taira, F. X. Kärtner, and A. R. Maier, "Spectral phase control of interfering chirped pulses for high-energy narrowband terahertz generation," Nat. Commun. **10**(1), 2591 (2019).
45. W.-M. Wang, P. Gibbon, Z.-M. Sheng, and Y.-T. Li, "Tunable circularly polarized terahertz radiation from magnetized gas plasma," Phys. Rev. Lett. **114**(25), 253901 (2015).
46. W. Shi, Y. J. Ding, N. Fernelius, and K. Vodopyanov, "Efficient, tunable, and coherent 0.18–5.27-THz source based on GaSe crystal," Opt. Lett. **27**(16), 1454–1456 (2002).
47. K. Imai, K. Kawase, J.-I. Shikata, H. Minamide, and H. Ito, "Injection-seeded terahertz-wave parametric oscillator," Appl. Phys. Lett. **78**(8), 1026–1028 (2001).
48. M. B. Agranat, S. I. Ashitkov, A. A. Ivanov, A. V. Konyashchenko, A. V. Ovchinnikov, and V. E. Fortov, "Terawatt femtosecond cr : forsterite laser system," Quantum Electron. **34**(6), 506–508 (2004).
49. M. Stillhart, A. Schneider, and P. Günter, "Optical properties of 4-n,n-dimethylamino-4^′-n^′-methyl-stilbazolium 2,4,6-trimethylbenzenesulfonate crystals at terahertz frequencies," J. Opt. Soc. Am. B **25**(11), 1914 (2008).
50. F. D. J. Brunner, O.-P. Kwon, S.-J. Kwon, M. Jazbinšek, A. Schneider, and P. Günter, "A hydrogen-bonded organic nonlinear optical crystal for high-efficiency terahertz generation and detection," Opt. Express **16**(21), 16496–16508 (2008).
51. C. Vicario, M. Jazbinsek, A. V. Ovchinnikov, O. V. Chefonov, S. I. Ashitkov, M. B. Agranat, and C. P. Hauri, "High efficiency THz generation in DSTMS, DAST and OH1 pumped by cr:forsterite laser," Opt. Express **23**(4), 4573–4580 (2015).
52. A. Majkić, M. Zgonik, A. Petelin, M. Jazbinšek, B. Ruiz, C. Medrano, and P. Günter, "Terahertz source at 9.4 THz based on a dual-wavelength infrared laser and quasi-phase matching in organic crystals OH1," Appl. Phys. Lett. **105**(14), 141115 (2014).
53. G. Montemezzani, M. Alonzo, V. Coda, M. Jazbinsek, and P. Günter, "Running electric field gratings for detection of coherent radiation," J. Opt. Soc. Am. B **32**(6), 1078–1083 (2015).
54. A. Schneider, "Theory of terahertz pulse generation through optical rectification in a nonlinear optical material with a finite size," Phys. Rev. A **82**(3), 033825 (2010).
55. A. S. Weling and D. H. Auston, "Novel sources and detectors for coherent tunable narrow-band terahertz radiation in free space," J. Opt. Soc. Am. B **13**(12), 2783–2792 (1996).
56. C. Ruchert, C. Vicario, and C. P. Hauri, "Scaling submillimeter single-cycle transients toward megavolts per centimeter field strength via optical rectification in the organic crystal OH1," Opt. Lett. **37**(5), 899 (2012).

Optics EXPRESS

57. E. A. Nanni, W. R. Huang, K.-H. Hong, K. Ravi, A. Fallahi, G. Moriena, R. J. D. Miller, and F. X. Kärtner, "Terahertz-driven linear electron acceleration," Nat. Commun. **6**(1), 8486 (2015).